Front. Struct. Civ. Eng. 2025, 19(6): 961–979
https://doi.org/10.1007/s11709-025-1185-4

RESEARCH ARTICLE

Shear behavior of reinforced concrete beams strengthened utilizing optimized external post-tensioning techniques

Mohamed GHALLA[a*], Alireza BAHRAMI[b*], Ehab MLYBARI[c], Moataz BADAWI[c]

[a] *Civil Engineering Department, Faculty of Engineering, Kafrelsheikh University, Kafrelsheikh 6860404, Egypt*
[b] *Department of Building Engineering, Energy Systems and Sustainability Science, Faculty of Engineering and Sustainable Development, University of Gävle, Gävle 801 76, Sweden*
[c] *Department of Civil Engineering, College of Engineering and Architecture, Umm Al-Qura University, Makkah 24382, Saudi Arabia*
[*] *Corresponding authors. E-mails: mohamed_shabaan@eng.kfs.edu.eg; alireza.bahrami@hig.se*

ABSTRACT The failure risk of defected reinforced concrete (RC) beams is considered a potential threat. This risk is experimentally identified, numerically analyzed, and thoroughly diminished to enhance structural safety and sustainability to mitigate the potential for structural collapse during construction. This research investigates the efficacy of an external post-tensioning mechanism in enhancing the behavior of defected RC beams lacking shear reinforcement, employing both experimental and numerical approaches. Fourteen RC beams were tested to evaluate the impact of post-tensioning force levels and the inclination angle of post-tensioning bars. The study found that regardless of force magnitude or angle, post-tensioning improved the failure characteristics of the non-stirrup beam. The failure mode transitioned from brittle to ductile, resulting in a more advantageous distribution of cracks. Reinforced beams exhibited increased cracking and ultimate loads, with the enhancement more pronounced at higher post-tensioning force levels. Inclined post-tensioning at angles of 75°, 60°, and 45° demonstrated substantial enhancement in cracking and ultimate loads, as well as elastic stiffness. The findings highlighted the superiority of inclined post-tensioning configurations, especially at 60°, for reinforced beams. Moreover, the study revealed a significant increase in absorbed energy with the proposed strengthening system. Additionally, finite element modelling (FEM) was used to replicate the tested beams. FEM accurately predicted the crack development, ultimate capacity, and deformation, aligning well with experimental observations.

KEYWORDS strengthening, external post-tensioning, reinforced concrete beam, finite element model, construction failure, risk mitigation

1 Introduction

The necessity for maintenance and repair arises in old reinforced concrete (RC) buildings owing to numerous factors such as catastrophic events, severe conditions, alterations in imposed loads, reinforcement corrosion, material aging, climate fluctuations, and inadequate maintenance [1–11]. Furthermore, suboptimal reinforcement detailing, like insufficient transverse reinforcement, heightens vulnerability, fostering brittle shear failure modes, which can compromise the structural integrity [12–16]. Consequently, to preserve the integrity of structures, strengthening emerges as the sole feasible solution. Addressing defects in RC beams through strengthening is crucial for mitigating failure risks and enhancing building safety and sustainability. However, careful consideration and management are essential to prevent the creation of secondary risks that could lead to construction failure. Numerous previous studies have

Article history: Received Nov 4, 2024; Accepted Feb 27, 2025

addressed critical issues in the design, behavior, and reinforcement of such RC structures [17–21]. These investigations have provided valuable insights into the structural integrity, durability, and performance under various loading conditions, contributing significantly to the advancement of engineering practices in this field [22–25].

Numerous studies have been conducted to explore the strengthening of RC beams employing diverse methods and materials. Traditional approaches, such as augmenting the beam section with RC jackets or utilizing externally attached steel elements, may be deemed structurally sound. However, they may fall short of meeting contemporary standards that often demand interventions characterized by both time and cost efficiency [26–33]. The primary drawbacks of concrete jacketing include the increase in section size and excessive weight. Conversely, the main disadvantages associated with steel jacketing are surface corrosion, operational challenges, and handling difficulties [34]. To address these challenges, innovative methods, for instance, the utilization of fiber reinforced polymers (FRP) materials, has emerged [35].

FRP may be employed to improve the shear capacity of concrete beams using various configurations, including side jacketing, U-shape wrapping, and full wrapping. Based on prior research [36–39], the most effective orientation was found to be full wrapping, followed by U-shaped and side configurations. However, it should be noted that this technique of reinforcement may be susceptible to premature FRP rupture, particularly along the corners of the beam.

Furthermore, the use of FRP shear strengthening can be made at various angles, with the 45° angle proving most effective due to its perpendicular alignment with the shear crack. Moreover, incorporating different layers of FRP has been instrumental in greatly enhancing both the ductility and shear capacity of strengthened beams [40–42].

FRP materials offer improved performance, simplified installation, increased durability, and time efficiency. However, FRP comes with notable drawbacks, primarily associated with its epoxy resin matrix. These limitations include suboptimal performance at high temperatures, potential debonding from concrete substrates, unsuitability for wet surfaces, and incompatibility with masonry [43–46]. This implies that the application of FRP may not be suitable for all scenarios, emphasizing the necessity for new techniques that can mitigate some of these drawbacks.

The utilization of external post-tensioning, where tendons are positioned outside the RC element, proves to be a potent method for both fortifying existing structures and facilitating the construction of new ones through a more streamlined process. The application of external tendons is characterized by its ability to be implemented without extensive manual labor, making it well-suited for installation in challenging and hard-to-reach areas [47,48].

Employing FRP tendons for the external post-tensioning of RC beams remarkably improved their flexural behavior, resulting in adequate crack patterns and increased ductility [49]. Notably, the flexural performance of RC beams externally pre-stressed using carbon FRP tendons was observed to be comparable to those of externally pre-stressed beams with steel tendons [50]. Nevertheless, the superior ductility of externally pre-stressed RC beams using glass FRP tendons, albeit with a lower carrying capacity than those pre-stressed with carbon FRP or steel tendons [51].

From the existing literature, it is evident that insufficient shear reinforcement may lead to an undesirable, brittle failure in RC beams. To prevent such failure, various techniques can be employed to strengthen these deficient beams, with external post-tensioning emerging as a promising method to address the limitations of conventional strengthening approaches. Despite some research focusing on the flexural enhancement of beams through external post-tensioning, there remains a scarcity of studies examining the utilization of this technique in enhancing the shear strength of RC beams. Consequently, the present study is dedicated to assessing the efficiency of an external post-tensioning mechanism in improving the performance of RC beams lacking adequate shear reinforcement.

2 Experimental investigation

2.1 Beam characteristics and test matrix

An experimental study involving fourteen RC beams was devised to explore the efficacy of employing the external post-tensioning technique to enhance the behavior of non-stirrup RC beams. The experimental study was structured into five groups, as outlined in Table 1. G1 involved two beams, serving as the reference. B0 exhibited no defects, while the second beam (UB) featured a non-stirrup zone lacking shear stirrups, as depicted in Fig. 1(b).

The other groups from G2 to G5 were formulated to examine the impact of the post-tensioning bars' angle corresponding to the longitudinal section of the beam. The studied angles were 90°, 75°, 60°, and 45°. Each group, excluding the control, included three RC beams subjected to three distinct levels of post-tensioning force, determined as a portion of the ultimate load (P_u) obtained from the control beam without defects. The applied post-tension force levels were $0.5P_u$, $0.75P_u$, and P_u. In Table 1, the beam ID is structured as follows: the first term (UB) refers to the non-stirrup beam, the second term signifies

Table 1 Details of tested beams

Group	Beam ID	Strengthening configuration	Post-tensioning level, P_P	Post-tensioning angle, q
G1	B0	control	–	–
	UB	defected	–	–
G2	UB	vertical post-tensioning technique	–	–
	UB-90-0.5P_u	vertical post-tensioning technique	50%P_u	90°
	UB-90-0.75P_u	vertical post-tensioning technique	75%P_u	90°
	UB-90-P_u	vertical post-tensioning technique	100%P_u	90°
G3	UB	inclined post-tensioning technique	–	–
	UB-75-0.5P_u	inclined post-tensioning technique	50%P_u	75°
	UB-75-0.75P_u	inclined post-tensioning technique	75%P_u	75°
	UB-75-P_u	inclined post-tensioning technique	100%P_u	75°
G4	UB	inclined post-tensioning technique	–	–
	UB-60-0.5P_u	inclined post-tensioning technique	50%P_u	60°
	UB-60-0.75P_u	inclined post-tensioning technique	75%P_u	60°
	UB-60-P_u	inclined post-tensioning technique	100%P_u	60°
G5	UB	inclined post-tensioning technique	–	–
	UB-45-0.5P_u	inclined post-tensioning technique	50%P_u	45°
	UB-45-0.75P_u	inclined post-tensioning technique	75%P_u	45°
	UB-45-P_u	inclined post-tensioning technique	100%P_u	45°

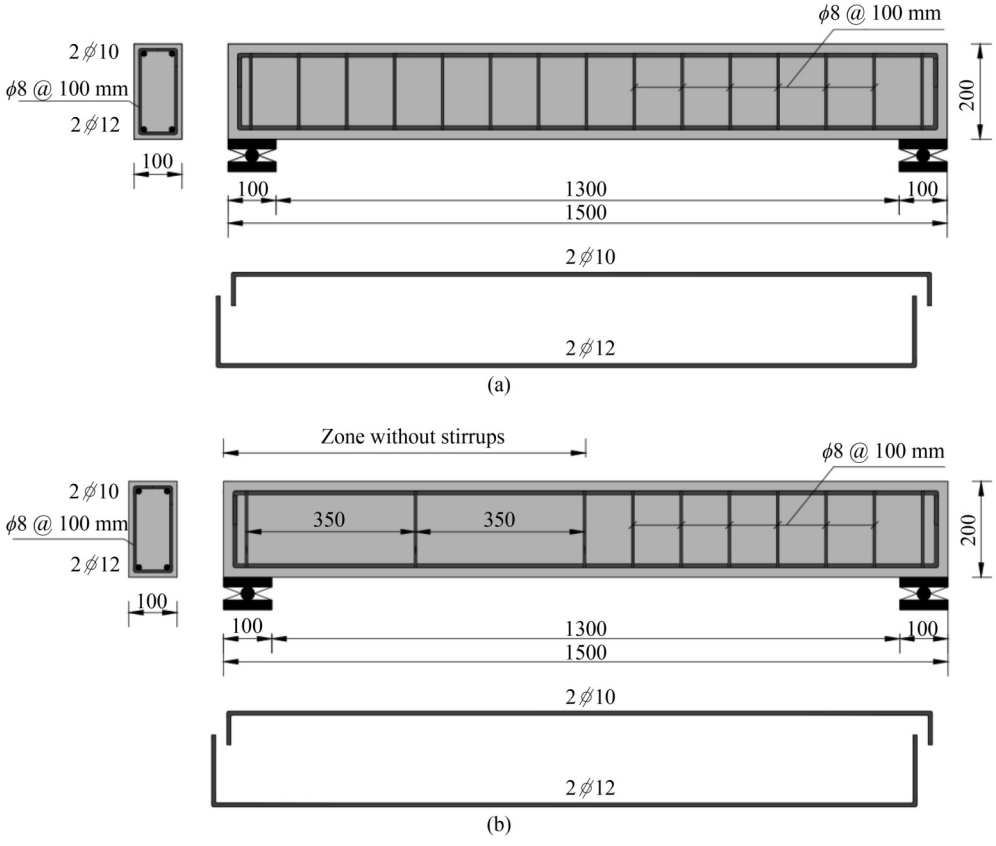

Fig. 1 Schematic and details of tested beams (unit: mm): (a) control beam; (b) non-stirrup beam.

the inclination angle of the post-tensioning steel bars (90°, 75°, 60°, and 45°), while the last term indicates the post-tension force level (0.5P_u, 0.75P_u, and P_u).

As displayed in Fig. 1, the examined beams possessed a 100 mm × 200 mm cross-section, a 1300 mm clear span, and total span of 1500 mm. Each beam underwent

reinforcement with two rebars, measuring 12 mm in diameter for bottom and 10 mm for top reinforcements. The control beam B0 was reinforced in shear using 8 mm stirrups spaced every 100 mm through its span, as shown in Fig. 1(a). For beam UB and the strengthened ones, 8 mm stirrups were aligned utilizing a 100 mm interval through their half span, while the other half was deficient in shear reinforcement except for one middle stirrup, employed for positioning the main bars, as demonstrated in Fig. 1(b). The decision to implement this approach aimed at minimizing the overall cost associated with strengthening such RC beams. Numerous investigators have used this approach [52–56]. For the strengthened RC beams, the post-tension load was applied externally through the installation of a 12 mm steel bar.

2.2 Properties of materials and mix composition

All beams were constructed using normal concrete (NC), comprising 350 kg/m^3 of ordinary Portland cement, 700 kg/m^3 of clean sand as fine aggregate, and 1150 kg/m^3 of dolomite as coarse aggregate, with a water to cement ratio of 0.42. NC cylinders, with dimensions of 150 mm in diameter and 300 mm in length, were fabricated using the identical batch employed for casting the RC beams to assess concrete compressive strength. Additionally, dog-boned samples, as displayed in Fig. 2, were cast and tested to determine concrete tensile strength. Moreover, the steel elements were tested with the same machine, as shown in Fig. 3. The achieved strengths in compression and tension were around 25 and 1.7 MPa, respectively. The stress–strain behavior is depicted in Fig. 4. Furthermore, the steel elements employed, including longitudinal reinforcement, stirrups, post-tensioning bars, and steel plates, underwent direct tensile testing, as illustrated in Fig. 3, for characterization. The obtained stress–strain responses, along with the idealized ones, are presented in Fig. 5.

2.3 Casting and preparation for strengthening

Figures 6 and 7 display the procedures for casting and strengthening. In the scenario of vertical post-tensioning (Fig. 6(a)), both bottom and top faces of the beam were adapted, following concrete hardening, at the locations of the steel plates, as depicted in Fig. 7(a). For beams equipped with inclined post-tensioning systems (Figs. 6(b)–6(d)), the bottom and top surfaces of the beam were adapted concerning the inclination angle of post-tensioned bars, as shown in Fig. 7(b). After surface adaptation, the steel plates were positioned, and the steel bars were installed to connect the top and bottom plates, as demonstrated in Fig. 7(c). Following this, steel nuts were applied to both ends of each bar and tightened to achieve the required post-tensioning level before testing.

It is worth mentioning that the practical application of the proposed strengthening technique can be implemented by drilling a groove into the upper side of the beam and installing the upper steel plate. The post-tensioning steel

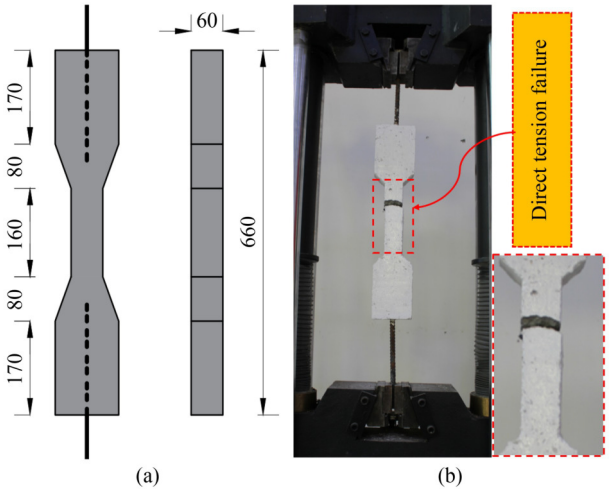

Fig. 2 Direct tensile test for NC (unit: mm): (a) sample dimensions; (b) test of specimen.

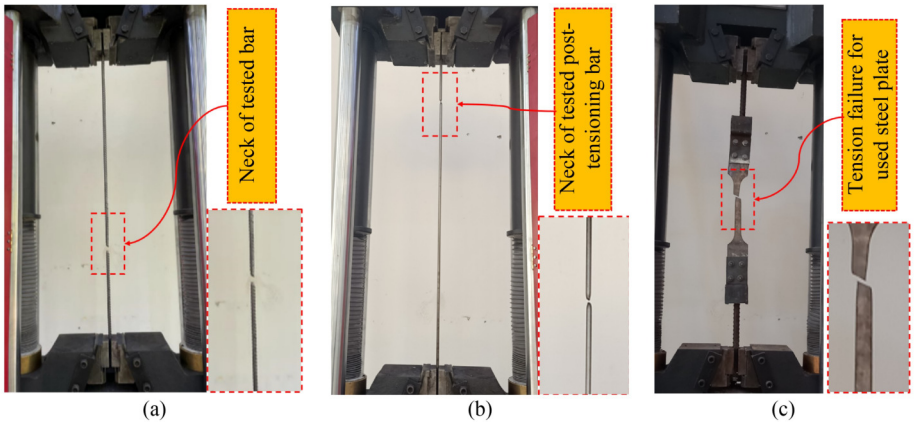

Fig. 3 Direct tensile tests for steel elements: (a) test of steel bar specimen; (b) test of post-tensioning bar specimen; (c) test of rigid steel plate specimen.

bars were passed to the lower steel plate, then the tensioning process was carried out with the specified tension stresses.

2.4 Loading arrangement, test arrangement, and instrumentation

The prepared beams were tested. All beams underwent testing through a three-point loading regimen (Fig. 8). To precisely gauge the utilized load, a calibrated load cell was employed. Concurrently, a linear variable differential transformer (LVDT) was strategically placed opposite the loading point to measure deflection. The load was operated through a displacement control regimen up to failure, and the entire load–deflection response was recorded throughout the loading stages.

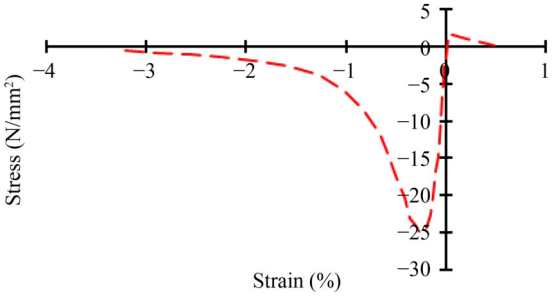

Fig. 4 Constitutive stress–strain behavior for NC.

3 Experimental results and discussion

3.1 Cracks inspection and modes of failure

For beam B0, the first flexural crack emerged at the middle under a load of 17.35 kN, constituting approximately 26% of its ultimate load. With the

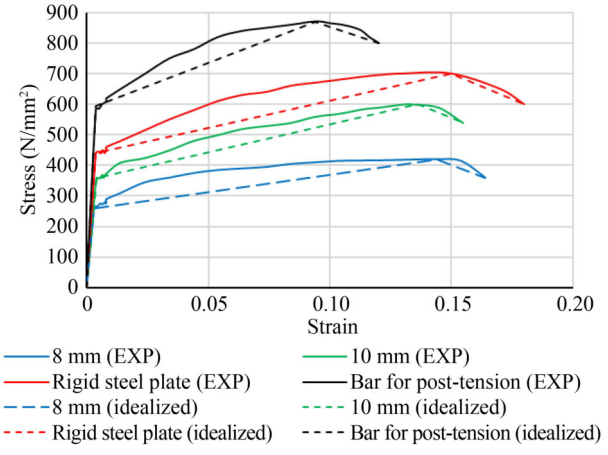

Fig. 5 Experimental and idealized uniaxial stress–strain responses for steel components (EXP: experimental).

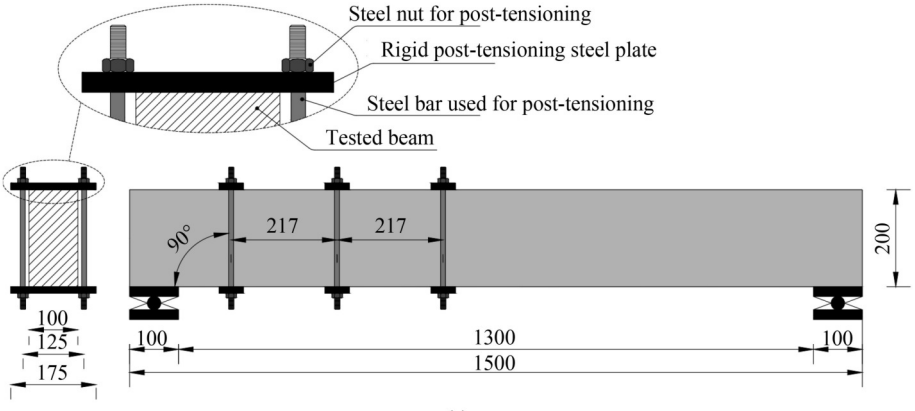

(a)

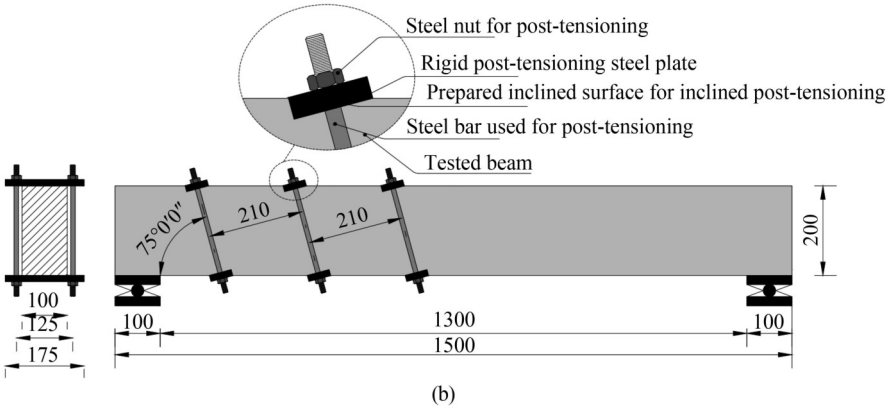

(b)

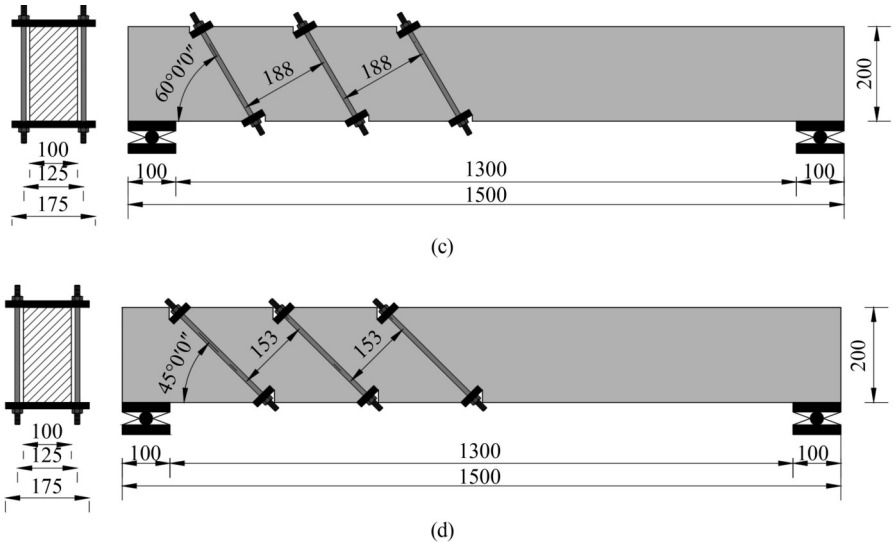

Fig. 6 Strengthening details (unit: mm): (a) G2 (vertical technique); (b) G3 (inclined with $\theta = 75°$); (c) G4 (inclined with $\theta = 60°$); (d) G5 (inclined with $\theta = 45°$).

Fig. 7 Strengthening preparation: (a) vertical post-tensioning adapting; (b) inclined post-tensioning adapting; (c) applying post-tensioning force.

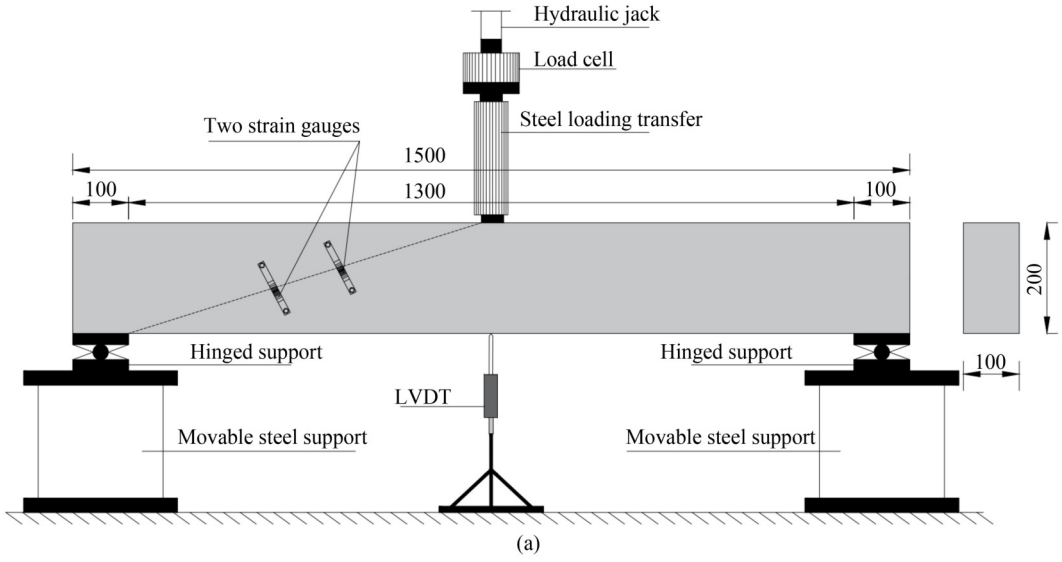

(a)

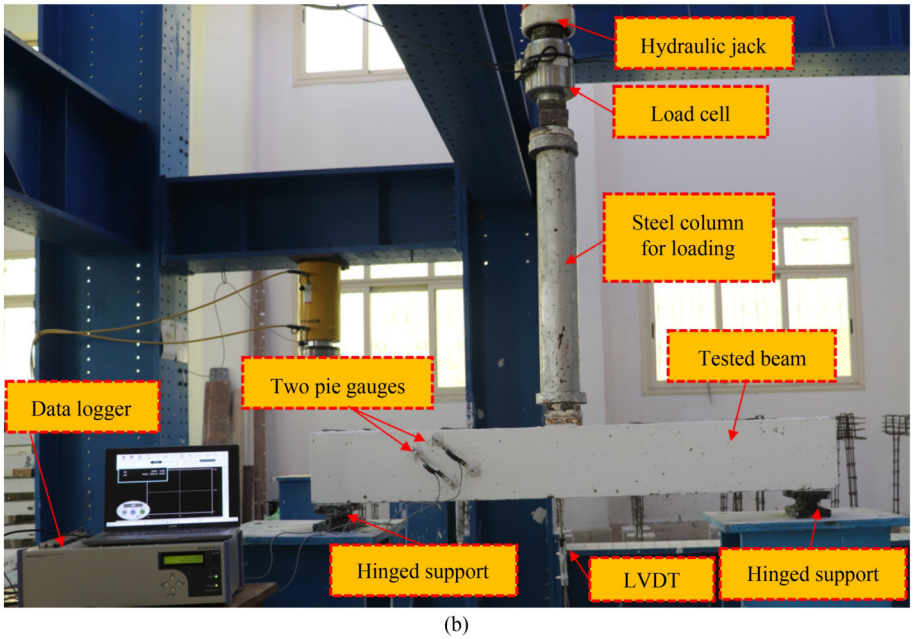

(b)

Fig. 8 Test arrangement and instrumentations (unit: mm): (a) schematic drawing; (b) actual test.

augmenting load, additional flexural cracks appeared and raised upward. The application of increasing loads, flexural-shear cracks initiated at both supports and extended to the loading point, as demonstrated in Fig. 9(a). Finally, the beam underwent flexural failure at a load of around 67.02 kN.

For the non-stirrup beam, UB, cracks originated in the shear zone, attributed to the absence of shear reinforcement, at approximately 11.56 kN (cracking load, P_{cr}), which was 33% lower than that of B0. As the load increased, additional cracks within the non-stirrup region appeared and propagated toward the loading point, as shown in Fig. 9(b). Shear failure was registered at a load of about 43.70 kN, representing a 35% drop compared to the reference beam. Figure 9(a) clearly indicates that, unlike the non-stirrup zone, no cracks were observed in the shear zone containing steel stirrups along its length.

The patterns of cracks observed in the beams belonging to G2, featuring a vertical post-tensioning system, are displayed in Fig. 10. Overall, a more favorable distribution of cracks was observed in this group in comparison to the non-stirrup beam. Flexural cracks initiated within the mid-span zone at 15.20, 17.50, and 19.80 kN for beams with post-tensioning forces of $0.5P_u$, $0.75P_u$, and P_u, respectively. Notably, the observed cracking load surpassed that of the non-stirrup beam for post-tensioning forces of $0.75P_u$ and P_u. With increasing load, more flexural cracks initiated and propagated upward, as represented in Fig. 10. For a post-tensioning force of $0.5P_u$, more cracks initiated in the shear non-stirrup zone, as shown in Fig. 10.

As the post-tensioning force increased, the cracks

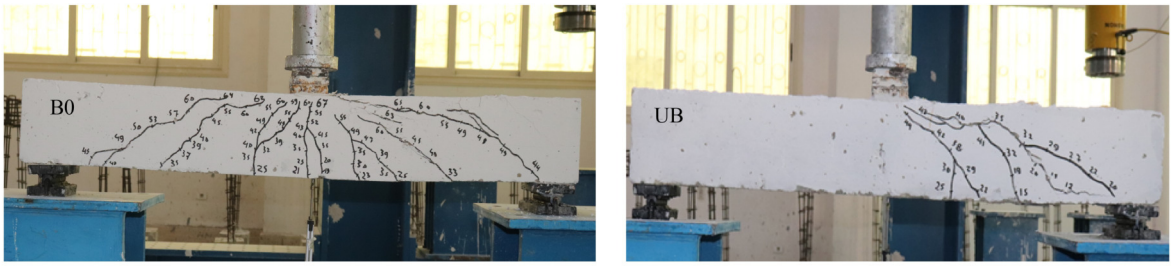

(a) (b)

Fig. 9 Crack patterns of G1: (a) control beam; (b) non-stirrup beam.

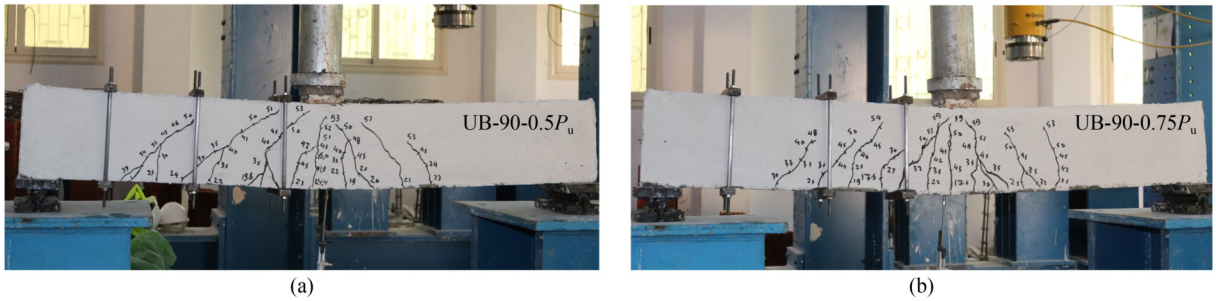

(a) (b)

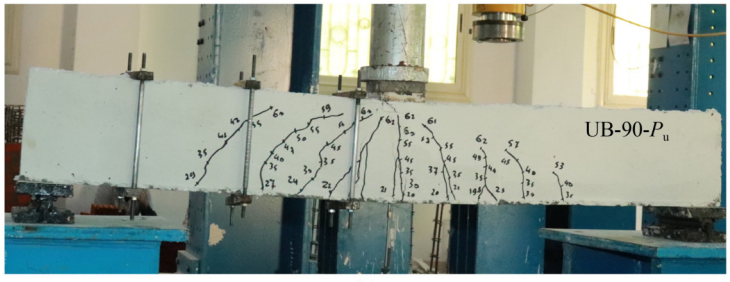

(c)

Fig. 10 Crack patterns of G2: (a) UB-90-0.5P_u; (b) UB-90-0.75P_u; (c) UB-90-P_u.

shifted toward the middle region, with a reduction in the shear region and wider spacing between cracks. All beams in this group exhibited flexural failure at 53.26, 59.11, and 62.65 kN for beams UB-90-0.5P_u, UB-90-0.75P_u, and UB-90-P_u, respectively.

Figure 11 illustrates the crack patterns observed in beams strengthened through the application of post-tensioning force at a 75° angle (G3). It is evident that the increase in the applied post-tensioning force enhanced crack distribution and compensated for the lack of internal stirrups. Flexural mid-span cracks initiated at critical loads of approximately 14.2, 15.80, and 21 kN for beams UB-75-0.5P_u, UB-75-0.75P_u, and UB-75-P_u, respectively.

At the lower post-tensioning level (0.5P_u), three main inclined cracks appeared within the non-stirrup shear zone, as displayed in Fig. 11(a). Elevating the post-tensioning level to 0.75P_u resulted in denser cracks shifted toward the middle zone compared to the lower post-tensioning level, as shown in Fig. 11(b). Further increasing the post-tensioning force (equivalent to P_u) led to appearing only two major cracks, attributed to stress concentration, in the non-stirrup shear zone at the contact zone between the steel plates and the beam. These two cracks propagated between the post-tensioned bars, as demonstrated in Fig. 11(c).

For beams belonging to G4, where the post-tensioning bars were inclined at 60°, the crack patterns are depicted in Fig. 12. Cracks originated at the middle region of the beam at loads of 22.5, 24, and 26.45 kN for beams UB-60-0.5P_u, UB-60-0.75P_u, and UB-60-P_u, respectively. These values represent 37.7%, 35.7%, and 35.9% of their P_u. With increasing load, cracks propagated upward, and more distributed cracks occurred along the bottom of the beam. Ultimately, all beams exhibited a flexural failure upon reaching their ultimate capacity. Remarkably similar crack patterns were observed in the shear zones on both sides of the beam (with and without stirrups), underscoring the efficacy of the suggested strengthening method.

The observed patterns of cracks in the beams of G5 are displayed in Fig. 13. Similar to previous strengthened groups, cracks initially originated within the mid-span zone and then progressed upward, as depicted in Fig. 13. As the applied load continued to increase, additional cracks began to form along the entire length of the beam.

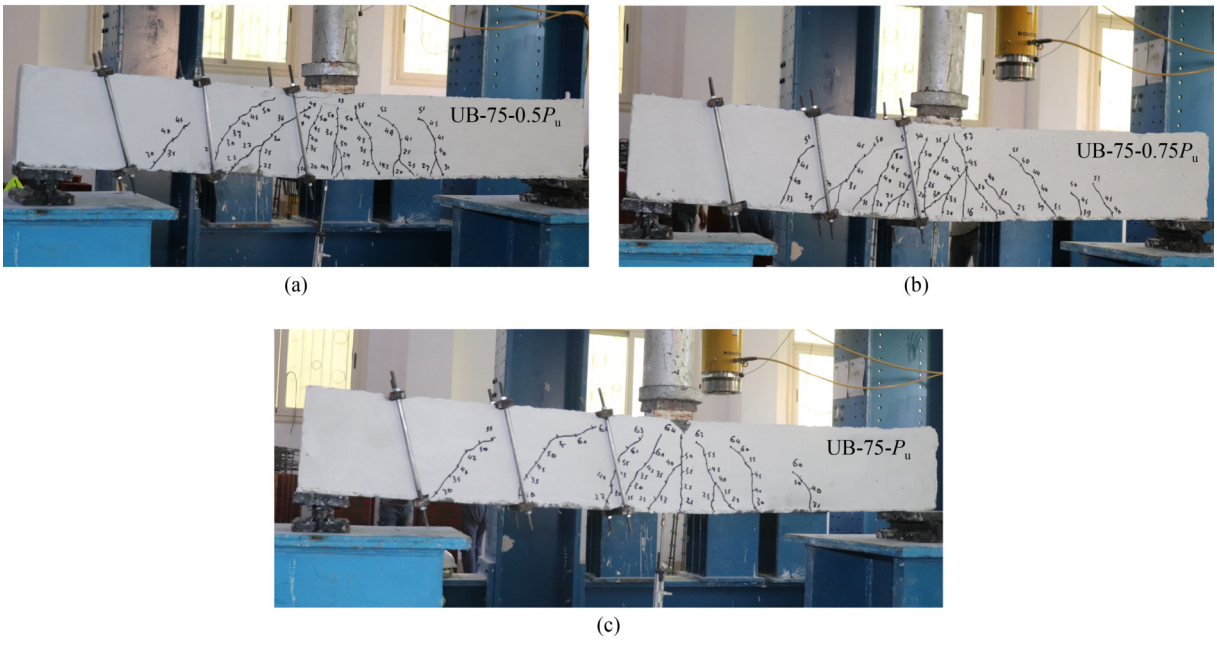

Fig. 11 Failure modes of G3: (a) UB-75-0.5P_u; (b) UB-75-0.75P_u; (c) UB-75-P_u.

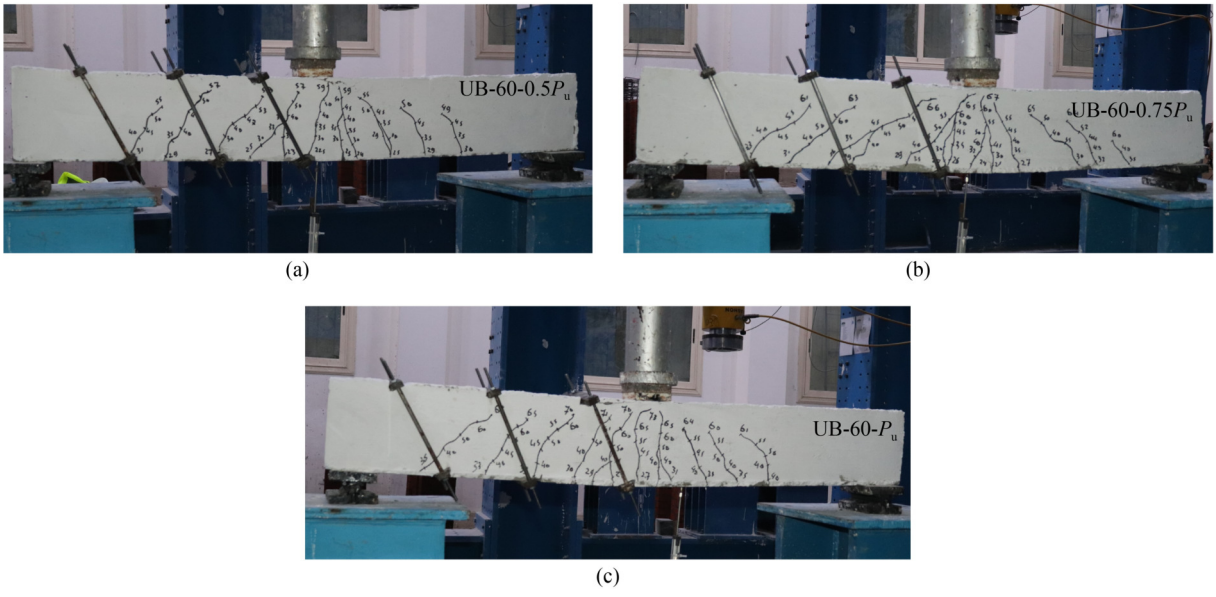

Fig. 12 Crack patterns of G4: (a) UB-60-0.5P_u; (b) UB-60-0.75P_u; (c) UB-60-P_u.

The recorded cracking loads were 19.5, 23.12, and 23.4 kN for beams UB-45-0.5P_u, UB-45-0.75P_u, and UB-45-P_u, respectively, constituting 31.2%, 35.1%, and 34.4% of their respective P_u.

Irrespective of the applied force magnitude and angle, the utilization of post-tensioning force improved the failure behavior of the non-stirrup beam. The failure mode was shifted from shear to either flexural or flexural shear, highlighting the effectiveness of employing this technique to compensate for the absence of shear reinforcement. Moreover, it was noted that the cracking load increased with greater post-tensioning forces.

3.2 Load–deflection characteristics

Figure 14 displays load against vertical mid-span deflection responses for all beams, while Table 2 provides recorded critical loading values and their corresponding mid-span deflections during loading stages. In Fig. 14(a), the absence of shear stirrups in UB led to a substantial decrease in stiffness and loads at cracking and ultimate stages compared to B0. When the cracking stage began, a reduction of approximately 33.4% in the load was witnessed, along with an increase in the deflection of about 13%. With increasing the load,

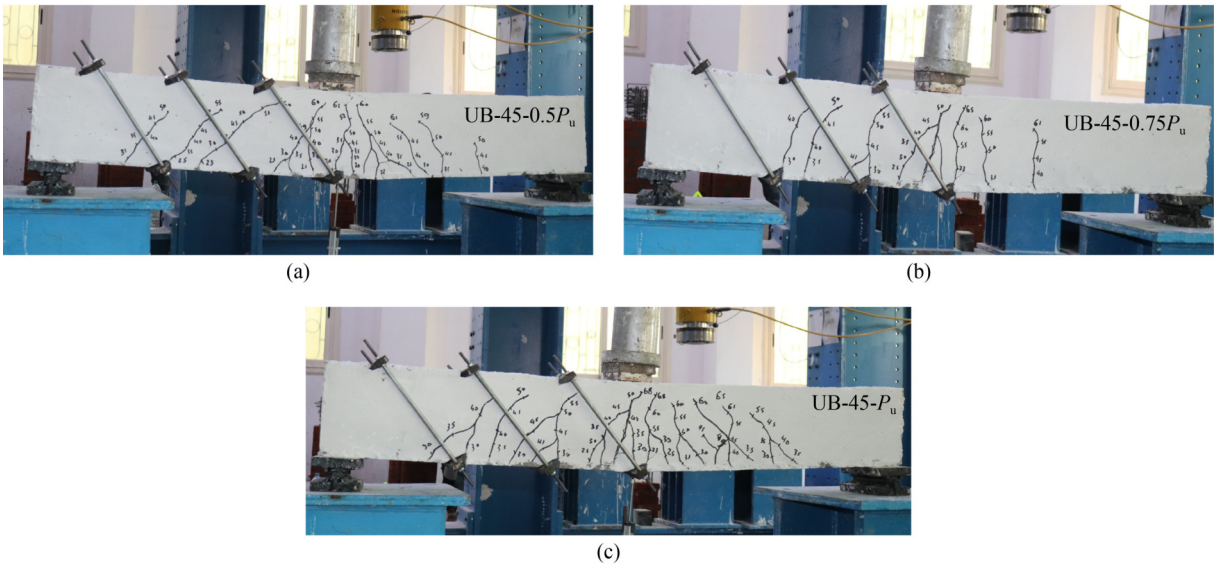

Fig. 13 Crack patterns of G5: (a) UB-45-0.5P_u; (b) UB-45-0.75P_u; (c) UB-45-P_u.

Table 2 Test results

Group	Beam ID	Cracking stage			Ultimate stage			Elastic stiffness index, K	K_B/K_{UB}	Absorbed energy, E	E_B/E_{UB}
		P_{cr} (kN)	P_{crB}/P_{crUB}	Δ_{cr} (mm)	P_u (kN)	P_{uB}/P_{uUB}	Δ_{Pu} (mm)				
G1	B0	17.35	1.50	2.05	67.02	1.53	20.17	8.46	1.70	1361.65	5.21
	UB	11.56	1.00	2.32	43.70	1.00	9.46	4.98	1.00	261.33	1.00
G2	UB	11.56	1.00	2.32	43.70	1.00	9.46	4.98	1.00	261.33	1.00
	UB-90-0.5P_u	15.20	1.31	2.42	53.26	1.22	14.25	6.28	1.26	536.18	2.05
	UB-90-0.75P_u	17.50	1.51	2.38	59.11	1.35	16.15	7.35	1.48	714.10	2.73
	UB-90-P_u	19.80	1.71	2.32	62.65	1.43	17.75	8.43	1.69	821.86	3.14
G3	UB	11.56	1.00	2.32	43.70	1.00	9.46	4.98	1.00	261.33	1.00
	UB-75-0.5P_u	14.20	1.23	2.52	55.82	1.28	17.59	5.63	1.13	745.55	2.85
	UB-75-0.75P_u	15.80	1.37	2.50	57.54	1.32	19.71	6.32	1.27	909.16	3.48
	UB-75-P_u	21.00	1.82	2.45	64.08	1.47	19.26	8.57	1.72	921.83	3.53
G4	UB	11.56	1.00	2.32	43.70	1.00	9.46	4.98	1.00	261.33	1.00
	UB-60-0.5P_u	22.50	1.95	2.55	59.65	1.36	16.69	8.82	1.77	873.61	3.34
	UB-60-0.75P_u	24.00	2.08	2.49	67.23	1.54	16.48	9.64	1.94	946.46	3.62
	UB-60-P_u	26.45	2.29	2.41	73.66	1.69	20.80	10.98	2.20	1371.73	5.25
G5	UB	11.56	1.00	2.32	43.70	1.00	9.46	4.98	1.00	261.33	1.00
	UB-45-0.5P_u	19.50	1.69	2.53	62.57	1.43	16.62	7.71	1.55	818.17	3.13
	UB-45-0.75P_u	23.12	2.00	2.51	65.83	1.51	15.22	9.21	1.85	988.91	3.78
	UB-45-P_u	23.40	2.02	2.40	68.05	1.56	17.01	9.75	1.96	1040.16	3.98

Notes: P_{cr}: cracking load; Δ_{cr}: vertical deflection corresponding to P_{cr}; P_u: ultimate load; Δ_{Pu}: vertical deflection corresponding to P_u; K: elastic stiffness; E: absorbed energy.

B0 exhibited a hardening feature prior to getting its extreme load, a manner not noted in UB which faced a brittle shear failure along the non-stirrup zone. The registered P_u of UB was 34.8% less than that of B0, with a stiffness approximately 41% lower. Additionally, B0 demonstrated a superior deformation capacity along the ultimate stage.

By employing the vertical post-tensioning technique, improvements were evident in all stages concerning the non-stirrup beam (UB). The average augmentation in the

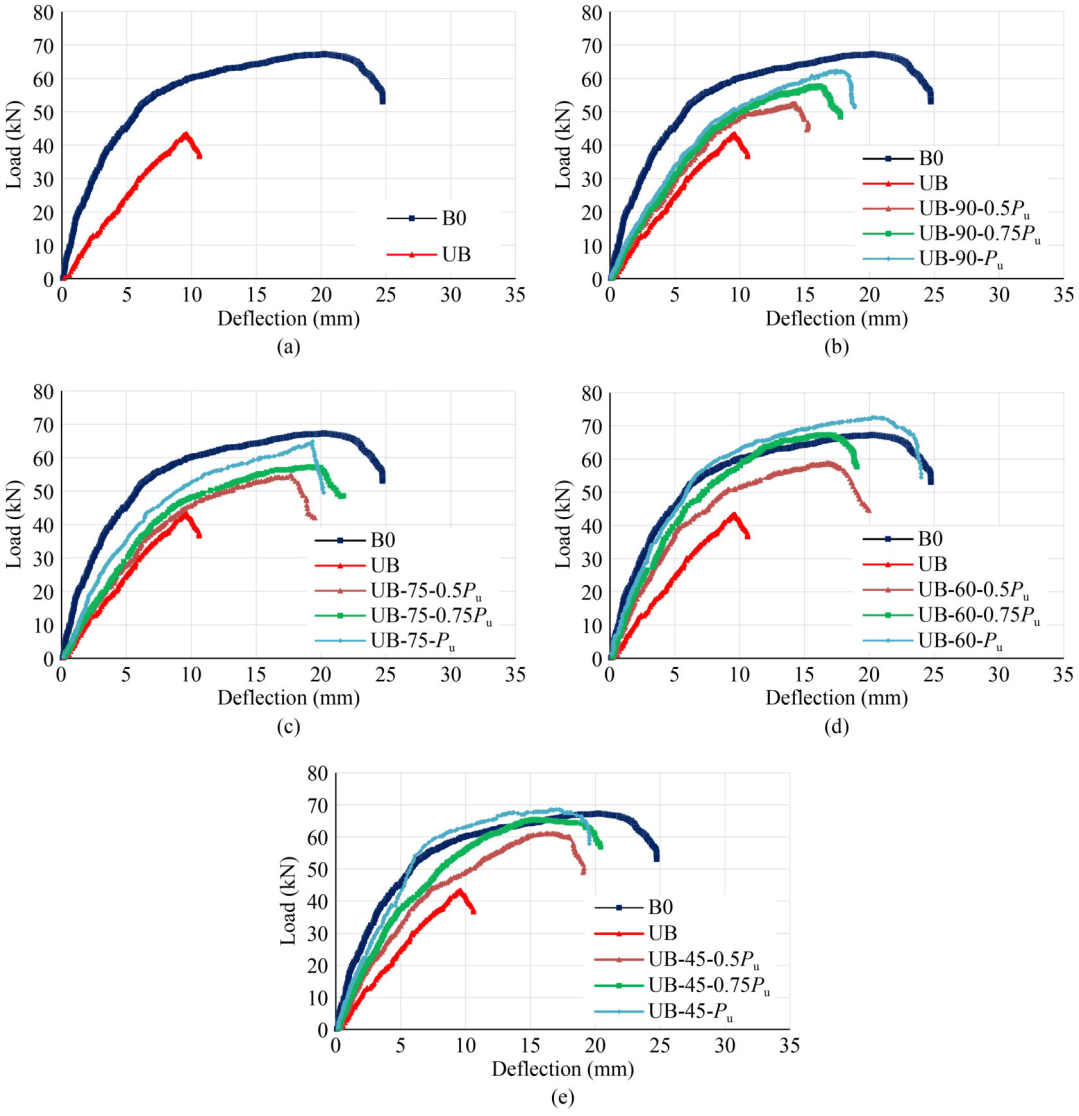

Fig. 14 Relationships between load and deflection for tested beams: (a) G1; (b) G2; (c) G3; (d) G4; (e) G5.

cracking load amounted to approximately 54.4%, while the average increase in the ultimate load reached about 33.5%. Furthermore, a hardening trend was observed before the ultimate stage in all strengthened beams, as illustrated in Fig. 14(b). Additionally, within this specific G2, the incremental application of post-tensioning levels marginally enhanced the elastic stiffness, cracking load, and ultimate load, thereby imparting greater ductility to the overall behavior. Despite these enhancements, it is noteworthy that all beams in this group exhibited an overall performance lower than that of B0.

The utilization of an inclined post-tensioning system for beam strengthening yielded a more enhanced load–deflection response. When contrasted with the non-strengthened beam, as outlined in Table 2, the average enhancements in the cracking load were 47%, 110%, and 90% for inclination angles of 75°, 60°, and 45°, respectively. Likewise, the enhancements in the ultimate capacity were 35%, 53%, and 50%, respectively, and concerning the elastic stiffness, they were 37%, 97%, and 79%. Based on the findings presented in Fig. 14 and Table 2, introducing an inclination to post-tensioned bars demonstrated superior performance in terms of load–deflection compared to vertical bars. The most significant improvement was noted when the provided angle was set at 60°, followed by 45° and then 75°. Moreover, across all three angles, augmenting the post-tensioning force resulted in a more pronounced enhancement in overall behavior. Applying a post-tensioning force equal to P_u could effectively compensate for the deficiency of shear reinforcement, particularly when the chosen angle was 60° or 45°.

The absorbed energy for each beam is depicted in Fig. 15. The findings demonstrate a noticeable enhancement in absorbed energy with the implementation of the proposed strengthening system. The most notable

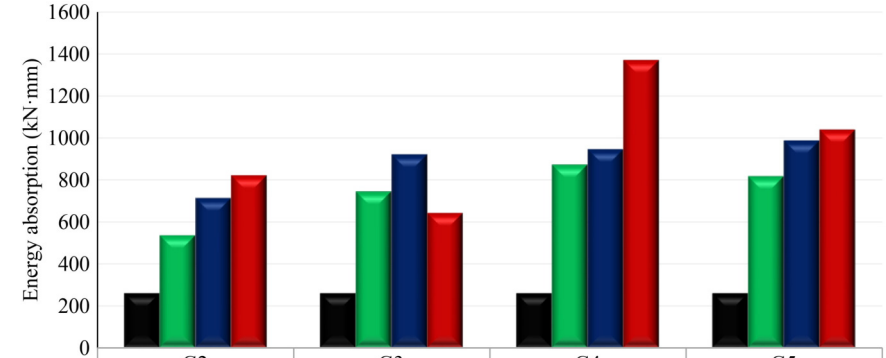

	G2	G3	G4	G5
UB	261.33	261.33	261.33	261.33
$0.5P_u$	536.18	745.55	873.61	818.17
$0.75P_u$	714.1	921.83	946.46	988.91
$1.00P_u$	821.86	642.39	1371.73	1040.16

Fig. 15 Measurement of energy absorption (unit: kN·mm).

enhancement was observed in G4, employing an inclination angle of 60°, followed by G5 with a 45° inclination. In addition, an increase in the post-tensioning force level resulted in an elevated absorbed energy, except for G3, where the optimal enhancement occurred at a post-tensioning force of $0.75P_u$. In comparison to the non-stirrup beam, there was an average increase of 164%, 229%, 307%, and 263% in absorbed energy for G2, G3, G4, and G5, respectively.

4 Numerical simulation

A distinctive aspect of numerical modeling is its ability to save time, money, and effort typically required for experimental testing [57–59]. This feature not only eases parametric investigations but also allows prediction of overall behavior. Abaqus, a commonly used tool based on the finite element approach, is legendary for its application in both static and dynamic, linear and nonlinear analyses [60]. We conducted a numerical study, through finite element modeling (FEM), utilizing the Abaqus software to scrutinize the behavior of RC beams with the non-stirrup zone, both strengthened and non-strengthened.

4.1 Models' built-up and interactions

The 8-node C3D8R element was employed in the modeling process. This element functioned as a representation for various components, including the steel elements utilized in the post-tensioning mechanism, as well as the plates for loading and supports, and RC beams, as displayed in Fig. 16. However, for depicting the stirrups and longitudinal bars, the 2-node T3D2 truss element was employed.

The contact between concrete and reinforcing steel, encompassing stirrups and longitudinal bars, was preserved as a comprehensive embedded constraint. In this configuration, concrete assisted as the host component, whereas the reinforcing steel acted as the embedded part. Furthermore, a complete bond was established within the RC beam and plates used for load and supports, as well as the rigid plates of the post-tensioning mechanism.

For the reference beams (G1), load was administered as a displacement to a reference point linked to the loading plate through a tie constraint. However, for the remaining groups, where beams underwent post-tensioning, the analysis unfolded in two distinct stages. Initially, post-tensioning stresses were assigned to the strengthening steel bars at a predetermined experimental value, as illustrated in Fig. 16(c). The subsequent step involved applying the displacement load to the load plate, mirroring the procedure for control beams.

4.2 Materials modeling

In the current FEM, the simulation of the behavior of NC was conducted using the concrete damage plasticity (CDP) model. CDP can replicate the inelastic tensile and compressive behaviors of concrete concerning tensile cracking and compressive crushing, which can be differentiated through damage assessment [61–66]. The model presented by Carreira and Chu [67] was utilized to replicate the nonlinear constitutive performance of NC. Equation (1) was employed to predict the stress–strain behavior in compression, while Eq. (2) characterizes the stress–strain behavior in tension.

$$\sigma_c = f_c \left[\frac{\beta\left(\frac{\varepsilon_c}{\varepsilon_{c0}}\right)}{\beta - 1 + \left(\frac{\varepsilon_c}{\varepsilon_{c0}}\right)^{\beta}} \right], \tag{1}$$

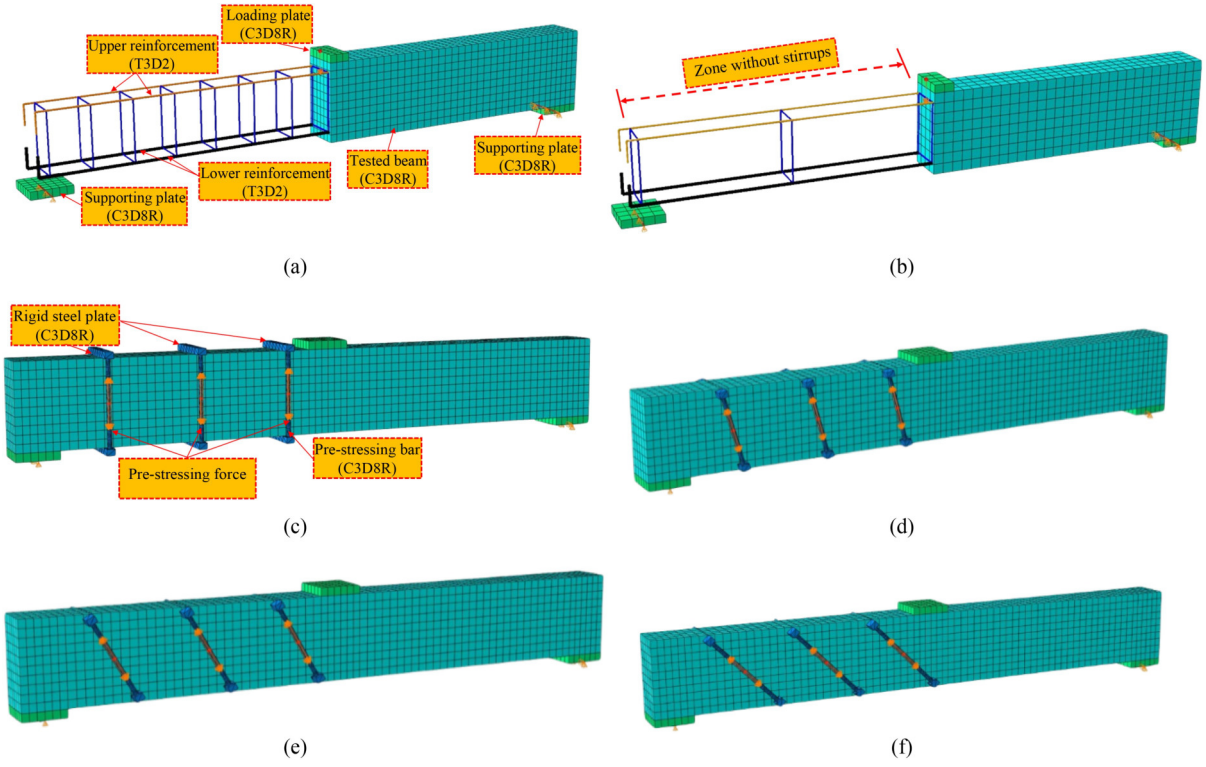

Fig. 16 Details of FEM: (a) B0; (b) UB; (c) UB-90-P_u; (d) UB-75-P_u; (e) UB-60-P_u; (f) UB-45-P_u.

$$\sigma_t = \begin{cases} f_t\left[1.2\dfrac{\varepsilon_t}{\varepsilon_{t0}} - 0.2\left(\dfrac{\varepsilon_t}{\varepsilon_{t0}}\right)^6\right], & 0 \leqslant \varepsilon_t \leqslant \varepsilon_{t0}, \\ f_t\left[\dfrac{\dfrac{\varepsilon_c}{\varepsilon_0}}{1.25\left(\dfrac{\varepsilon_t}{\varepsilon_{t0}} - 1\right)^2 - \dfrac{\varepsilon_t}{\varepsilon_{t0}}}\right], & \varepsilon_{t0} < \varepsilon_t. \end{cases} \tag{2}$$

In this case, the concrete stress and strain are represented by σ_c and ε_c, respectively, while the peak compressive stress and strain are designated by f_c and ε_{co}. Equation (3) can be used to ascertain the factor β, which is obtained depending on the stress–strain curve shape:

$$\beta = \left(\frac{f_c}{32.4}\right) + 1.55. \tag{3}$$

Within the outline of CDP (Eqs. (4) and (5)), the compression damage parameter (d_c) rest on both the total compressive strain (ε_c) and the plastic strain (ε_{Plc}). Likewise, the tension damage parameter (d_t) is established by its relationship with the total tensile strain (ε_t) and the cracking strain (ε_{Plt}). For reference, the idealized tensile stress–strain relations for NC can be understood from Fig. 4.

$$d_c = 1 - \frac{\sigma_c}{E_0(\varepsilon_c - \varepsilon_c^{pl})}, \tag{4}$$

$$d_t = 1 - \frac{\sigma_t}{E_0(\varepsilon_t - \varepsilon_t^{pl})}. \tag{5}$$

A sensitivity study was performed to fine-tune the parameters of the CDP model, yielding a dilation angle (ψ) set at 25° [68]. Furthermore, the remaining parameters of the CDP model were chosen in accordance with the default values recommended by Abaqus [69–72]. Additionally, following guidelines of Abaqus, the flow potential eccentricity (e) was set to 0.1, the biaxial to uniaxial compressive strength ratio (f_{b0}/f_{c0}) to 1.16, the ratio (K_c) to 0.667, and the viscosity parameter (μ) to 0.001.

The mesh size and type mark the accuracy of the FEM outcomes. Therefore, a parametric investigation was accomplished for the simulation of UB to evaluate the influence of the mesh type. Two key types of elements were used: C3D8 and C3D4 (a 4-node linear tetrahedral element). Figure 17(a) illustrates the influence of the mesh type on the load–deflection, obviously demonstrating the appropriateness of utilizing C3D8 elements for the numerical investigation of such beams. Moreover, the investigation of the mesh sensitivity was done for the same beam. Three different sizes reflected 15 mm × 15 mm, 30 mm × 30 mm, and 45 mm × 45 mm. It was found that a mesh size of 15 mm × 15 mm is appropriate when reflecting the analysis time spent, as displayed in Fig. 17(b).

The elasto-plastic model incorporating hardening was used to simulate the response of the reinforcing steel,

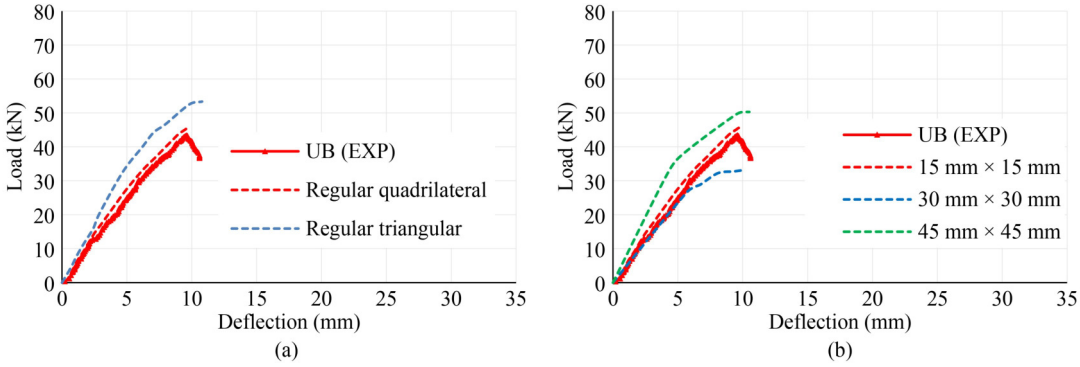

Fig. 17 Effects of mesh sensitivity on load–deflection curve of UB: (a) effect of regularity in case of mesh size 15 mm × 15 mm; (b) effect of variation in mesh size.

including both stirrups and reinforcing bars, as well as the bars employed for post-tensioning and their associated supporting plates. The model was constructed using the results obtained from direct tensile testing, as depicted in Fig. 5, which indicates the real and idealized uniaxial stress–strain responses for steel components.

4.3 Finite element model results

The FEM results underwent validation against experimental findings, specifically focusing on the load–deflection (Fig. 18) and crack outlines (Fig. 19). The outcomes indicated that FEM accurately predicted various aspects, including cracking, ultimate load capacity, and deflection across all stages. To clarify further, Table 3 presents an evaluation of the FEM outcomes concerning key points, such as cracking and ultimate load, along with their corresponding deflections, compared to experimental data. Along cracking, the average ratios of the predicted FEM cracking load to the experimentally monitored load, as well as their corresponding deflection ratios, were 1.03 and 0.98, respectively. The standard deviation (SD) values for these ratios were 0.008 and 0.0098, with coefficient of variation (COV) values of 0.0008 and 0.00098, respectively. In the final phase, the mean load and deflection ratios were 1.03 and 0.97, respectively. The SD values stood at 0.009 and 0.012, while the COV values were 0.0009 and 0.0012, respectively (Table 3).

Additionally, Fig. 19 displays that FEM effectively simulated numerous failure patterns and crack propagation detected experimentally. Figures 19(a) and 19(b) demonstrate the flexural failure of the reference beam and the brittle shear failure of the non-stirrup beam, respectively. In addition, FEM accurately represented the impact of the post-tensioning mechanism on the failure of strengthened beams, as depicted in Fig. 19.

5 Analytical study

This section presents an analytical approach for predicting the total shear resistance (q_{sh}) of RC beams that were shear-strengthened using an external post-tensioning technique. A theoretical expression (Eq. (6)) is introduced to evaluate the joint effects of these strengthening components [73,74]. The expression divides the shear resistance into three main constituents. 1) q_c, which signifies the essential shear resistance of the original RC beam, considering its material characteristics and existing geometry. Details for this calculation are provided in Eq. (7). 2) q_{stir}, which accounts for the added shear resistance from the current stirrups within the beam. The calculation for this involvement is detailed in Eq. (8). 3) q_{pt}, which reflects the specific contribution of the post-tensioning bars to the whole shear resistance of the strengthened beam. Further data on evaluating this component can be obtained from Eq. (9). The total shear force can be achieved from Eq. (10).

$$q_{sh} = q_c + q_{stir} + q_p, \tag{6}$$

$$q_c = \begin{cases} 0.16\sqrt{f_c'} + 17\rho_w \dfrac{V_u d}{M_u}, & \text{without post-tensioning force,} \\ \left(0.16\sqrt{f_c'} + 17\rho_w \dfrac{V_u d}{M_u}\right)\left(1 + \dfrac{2P_p}{14bS_p}\right), & \text{with post-tensioning force,} \end{cases} \tag{7}$$

$$q_{stir} = \frac{nA_{stir}f_{y,stir}}{bS_{stir}}, \tag{8}$$

$$q_p = \frac{2A_p f_{y,p}}{bS_p}(\cos\theta + \sin\theta), \tag{9}$$

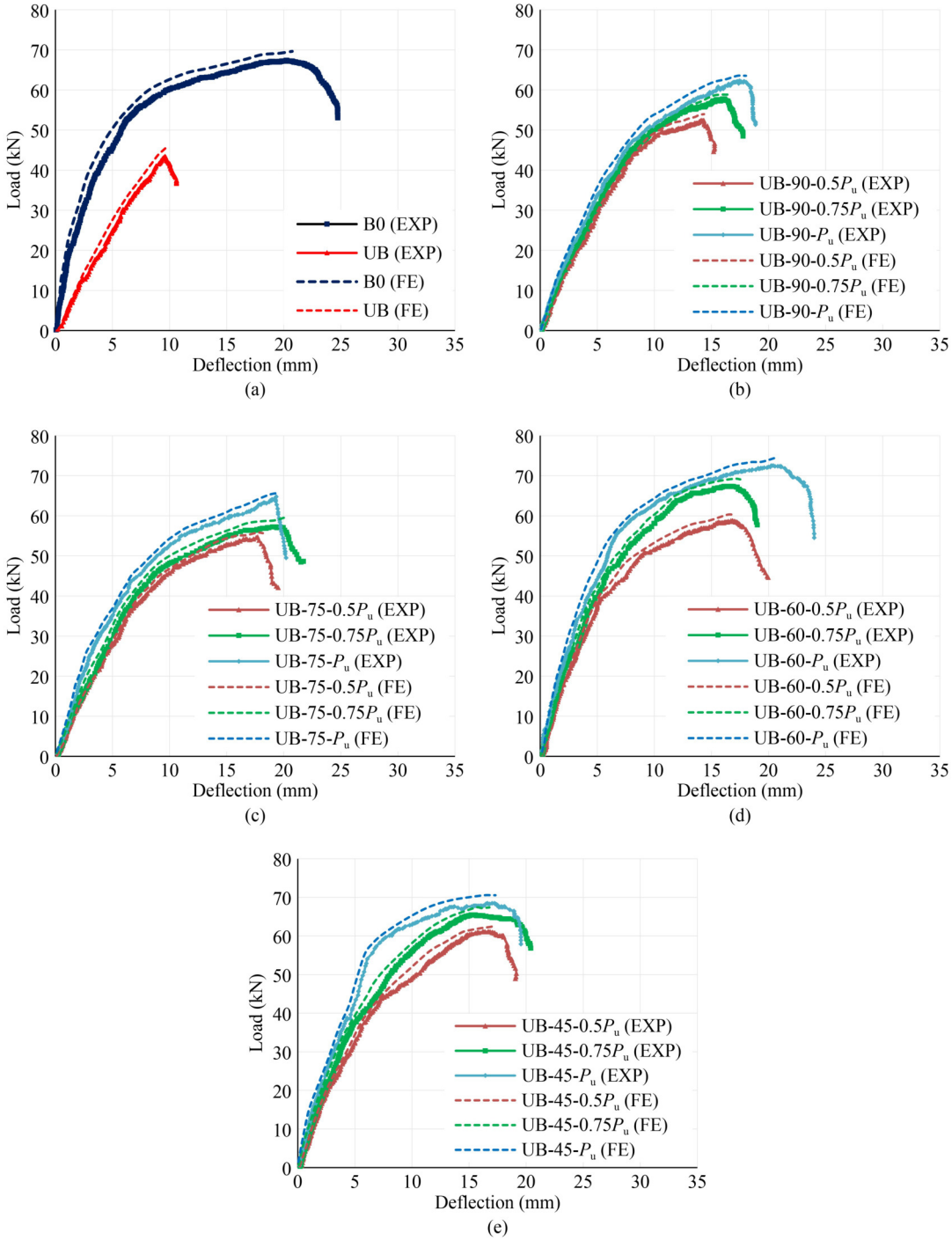

Fig. 18 Experimental and numerical load–deflection responses: (a) G1; (b) G2; (c) G3; (d) G4; (e) G5.

$$P_{sh} = 2 \times q_{sh} \times b \times d, \tag{10}$$

where q_{sh} is total shear strength obtained by the RC beam section; q_c is shear strength obtained by concrete; q_{stir} is shear strength obtained by stirrups; q_p is shear strength obtained by post-tensioning bars; ρ_w is flexural reinforcement ratio defined as $\rho_w = \frac{A_s}{bd}$; V_u and M_u are shear force and bending moment, respectively; $\frac{V_u d}{M_u} = \frac{1}{a/d}$, where a/d represents the shear span-to-depth ratio; P_p is the applied post-tensioning force per bar; b is the width of beam; S_p is the spacing of post-tensioning bars; n is the number of stirrup branches; A_{stir} is the cross-sectional area of the stirrup steel; $f_{y,stir}$ is the yield strength of the stirrup steel; S_{stir} is spacing between stirrups; A_p is the cross-sectional area of one post-tensioning bar; $f_{y,p}$ is the yield strength of the post-tensioning bar; θ is the inclination angle of the post-tensioning bar; d is the effective depth of the beam cross-section.

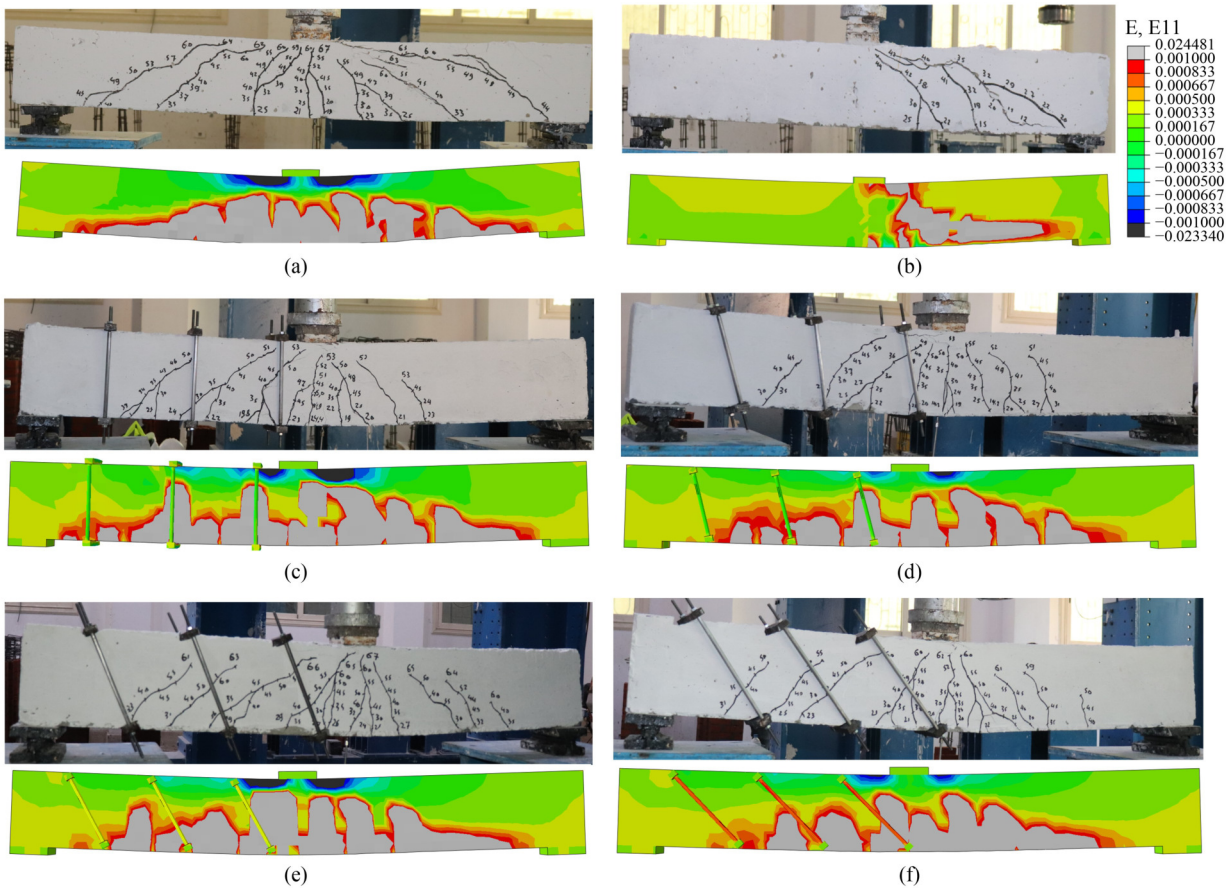

Fig. 19 FEM results: (a) control beam; (b) non-stirrup beam; (c) G2; (d) G3; (e) G4; (f) G5.

Table 3 A comparative analysis of numerical findings and experimental outcomes

Beam ID	P_{cr}			Δ_{cr}			P_u			Δ_{Pu}		
	EXP (kN)	FE (kN)	FE/EXP	EXP (mm)	FE (mm)	FE/EXP	EXP (kN)	FE (kN)	FE/EXP	EXP (mm)	FE (mm)	FE/EXP
B0	17.35	18.01	1.04	2.05	2.01	0.98	67.02	69.25	1.03	20.17	19.08	0.95
UB	11.56	12.12	1.05	2.32	2.25	0.97	43.70	45.19	1.03	9.46	9.25	0.98
UB-90-0.5P_u	15.20	15.85	1.04	2.42	2.33	0.96	53.26	55.23	1.04	14.25	13.98	0.98
UB-90-0.75P_u	17.50	17.62	1.01	2.38	2.31	0.97	59.11	62.12	1.05	16.15	15.75	0.98
UB-90-P_u	19.80	20.25	1.02	2.32	2.27	0.98	62.65	64.03	1.02	17.75	17.03	0.96
UB-75-0.5P_u	14.20	14.53	1.02	2.52	2.48	0.98	55.82	57.12	1.02	17.59	17.21	0.98
UB-75-0.75P_u	15.80	16.28	1.03	2.50	2.44	0.98	57.54	59.51	1.03	19.71	18.76	0.95
UB-75-P_u	21.00	21.64	1.03	2.45	2.37	0.97	64.08	65.98	1.03	19.26	18.33	0.95
UB-60-0.5P_u	22.50	23.05	1.02	2.55	2.50	0.98	59.65	61.08	1.02	16.69	16.12	0.97
UB-60-0.75P_u	24.00	24.86	1.04	2.49	2.46	0.99	67.23	68.85	1.02	16.48	16.03	0.97
UB-60-P_u	26.45	27.11	1.02	2.41	2.35	0.98	73.66	75.25	1.02	20.80	19.65	0.94
UB-45-0.5P_u	19.50	20.16	1.03	2.53	2.46	0.97	62.57	64.23	1.03	16.62	16.05	0.97
UB-45-0.75P_u	23.12	23.95	1.04	2.51	2.39	0.95	65.83	66.86	1.02	15.22	14.96	0.98
UB-45-P_u	23.40	24.02	1.03	2.40	2.36	0.98	68.05	70.12	1.03	17.01	16.52	0.97

Note: EXP: experimental; FE: finite element.

6 Conclusions

This research endeavors to examine, both experimentally and numerically, the efficiency of an external post-tensioning mechanism in enhancing the shear performance of defected RC beams, which participated in alleviating the risk severity of these RC beams. Fourteen RC beams underwent investigation, and the effects of post-tensioning force levels and the inclination angle of post-tensioning bars were evaluated. The conclusions derived from the results are as follows.

1) The utilization of post-tensioning force enhanced the failure characteristics of the non-stirrup beam. The failure mode transitioned from shear to either flexural or flexural shear. This underscored the efficacy of employing this technique to address the deficiency of shear reinforcement.

2) In contrast to the unreinforced beam, there were average improvements of 47%, 110%, and 90% in the cracking load for inclination angles of 75°, 60°, and 45°, respectively. Similarly, the increases in the ultimate loads were 35%, 53%, and 50%, respectively.

3) The application of an inclined post-tensioning system for beam reinforcement resulted in a superior load–deflection response compared to vertical configurations. The most notable enhancement was observed when the inclination angle was set at 60°, followed by 45° and then 75°.

4) Employing a post-tensioning force equivalent to P_u proved to be an effective means of compensating for the lack of shear reinforcement, especially when the selected angle was either 60° or 45°.

5) The findings demonstrated a considerable increase in absorbed energy with the application of the suggested strengthening system. The most remarkable improvement was noted in G4, utilizing an inclination angle of 60°.

6) FEM precisely predicted various aspects, encompassing crack development, ultimate capacity, and deflection throughout all phases.

Funding note Open access funding provided by University of Gävle.

Competing interests The authors declare that they have no competing interests.

References

1. Zheng A, Li S, Zhang D, Yan Y. Shear strengthening of RC beams with corrosion-damaged stirrups using FRP grid-reinforced ECC matrix composites. Composite Structures, 2021, 272: 114229
2. Abdallah A M, Badawi M, Elsamak G, Hu J W, Mlybari E A, Ghalla M. Strengthening of RC beams with inadequate lap splice length using cast-*in-situ* and anchored precast ECC ferrocement layers mitigating construction failure risk. Case Studies in Construction Materials, 2024, 20: e02747
3. Mo Z, Qiu J, Xu H, Xu L, Hu Y. Flexural and longitudinal shear performance of precast lightweight steel–ultra-high performance concrete composite beam. Frontiers of Structural and Civil Engineering, 2023, 17(5): 704–721
4. Sengun K, Arslan G. Investigation of the parameters affecting the behavior of RC beams strengthened with FRP. Frontiers of Structural and Civil Engineering, 2022, 16(6): 729–743
5. Khalilzadehtabrizi S, Sadaghian H, Farzam M. Uncertainty of concrete strength in shear and flexural behavior of beams using lattice modeling. Frontiers of Structural and Civil Engineering, 2023, 17(2): 306–325
6. El-Mandouh M A, Hu J W, Shim W S, Abdelazeem F, Elamak G. Torsional improvement of RC beams using various strengthening systems. Buildings, 2022, 12(11): 1776
7. Rageh B O, Elsamak G, Almaadawy A H, Elmasry A H. Parametric study on the behavior of thin-walled castellated beams subjected to static monotonic loading using finite-element analysis. Asian Journal of Civil Engineering, 2023, 24(4): 1041–1053
8. El-Zareef M A, Ghalla M, Hu J W, El-Demerdash W E. Damage detection of lightweight concrete dual systems reinforced with GFRP bars considering various building heights and earthquake intensities. Case Studies in Construction Materials, 2024, 20: e03191
9. Ghalla M, Mansour W, Li W, Wang P, Badawi M, El-Zareef M A. Enhancing the punching performance of two-way RC flat slabs using different configurations of embedded aluminum sections: Experimental program and numerical analysis. Construction and Building Materials, 2024, 434: 136737
10. Mansour W, Li W, Ghalla M, Badawi M, El-Zareef M A. Improving the punching capacity of two-way RC flat slabs via external strengthening using various configurations of aluminum sheets. Construction and Building Materials, 2024, 420: 135611
11. Fayed S, Ghalla M, Hu J W, Mlybari E A, Albogami A, Yehia S A. Shear strengthening of RC beams using prestressed near-surface mounted bars reducing the probability of construction failure risk. Materials, 2024, 17(23): 5701
12. Muttoni A, Ruiz M F. Shear strength of members without transverse reinforcement as function of critical shear crack width. ACI Structural Journal, 2008, 105(2): 163–172
13. Autrup F, Joergensen H B. Shear capacity of RC members without shear reinforcement: A modified crack sliding model. Engineering Structures, 2021, 239: 112147
14. Emara M, Salem M A, Mohamed H A, Shehab H A, El-Zohairy A.

Shear strengthening of reinforced concrete beams using engineered cementitious composites and carbon fiber-reinforced polymer sheets. Fibers, 2023, 11(11): 98

15. Alharthai M, Bahrami A, Badawi M, Ghalla M, Elsamak G, Abdelmgeed F A. Numerical study on enhancing shear performance of RC beams with external aluminum alloy plates bonded using steel anchors. Results in Engineering, 2024, 22: 102143
16. Emara M, Elsamak G, Ghalla M, Hu J W, Badawi M, Salama M I. Shear improvement of defected RC beams with sustainable aluminum boxes incorporating high performance concretes. Case Studies in Construction Materials, 2024, 21: e03500
17. Al-Smadi Y M, Al-Huthaifi N, Alkhawaldeh A A. The effect of longitudinal hole shape and size on the flexural behavior of RC beams. Results in Engineering, 2022, 16: 100607
18. Alhassan M, Alkhawaldeh A, Betoush N, Sawalha A, Amaireh L, Onaizi A. Harmonizing smart technologies with building resilience and sustainable built environment systems. Results in Engineering, 2024, 22: 102158
19. Al-Huthaifi N, Alkhawaldeh A A, Obaidat Y T, Alkhawaldeh M A. Flexural Strengthening of reinforced concrete beams with longitudinal circular hole using near-surface mounted CFRP strips. Practice Periodical on Structural Design and Construction, 2021, 27(2): 04021079
20. El-Zareef M A, El-Madawy M E. Optimization of infill panel for seismic response of multi-story RC frame buildings utilizing multi criteria optimization technique. Bulletin of Earthquake Engineering, 2018, 16(10): 4951–4970
21. El-Zareef M A. An experimental and numerical analysis of the flexural performance of lightweight concrete beams reinforced with GFRP bars. Engineering, Technology & Applied Scientific Research, 2023, 13(3): 10776–10780
22. El-Zareef M A, Abdulrahaman A G, Alnemari A. Experimental investigation of punching shear behaviour of ultra-high performance self-compacting concrete slabs. Case Studies in Construction Materials, 2023, 19: e02307
23. El-Zareef M A. Seismic damage assessment of multi-story lightweight concrete frame buildings reinforced with glass-fiber rods. Bulletin of Earthquake Engineering, 2017, 15(4): 1451–1470
24. Alkhawaldeh A A, Alhassan M A, Elrefae A. A case study of implementing life cycle cost analysis in sustainability assessment. In: Proceedings of the 2022 International Arab Conference on Information Technology (ACIT). Abu Dhabi: IEEE, 2022
25. Al-Baijat H, Alhawamdeh M, Khawaldeh A. Studying the flexural behavior of reinforced concrete beams under the effect of high temperature: A finite element model. Advances in Science and Technology Research Journal, 2019, 13(2): 150–156
26. Waghmare S P B. Materials and jacketing technique for retrofitting of structures. International Journal of Advanced Engineering Research and Studies, 2011, 1(1): 15–19
27. Raval S S, Dave U V. Effectiveness of various methods of jacketing for RC beams. Procedia Engineering, 2013, 51: 230–239
28. Aldhafairi F, Hassan A, Abd-EL-Hafez L M, Abouelezz A E Y. Different techniques of steel jacketing for retrofitting of different types of concrete beams after elevated temperature exposure. Structures, 2020, 28: 713–725
29. Sharaky I A, Mohamed H A, Torres L, Emara M. Flexural behavior of rubberized concrete beams strengthened in shear using welded wire mesh. Composite Structures, 2020, 247: 112485
30. Ahmed S, Mohamed E Y, Mohamed H A, Emara M. Experimental and numerical investigation of flexural behavior of RC beams retrofitted with reinforced UHPFRC layer in tension surface. Structures, 2023, 49: 106–123
31. Amirabad N G, Alaee F J, Jalali M. Ductility improvement of GFRP-RC beams using precast confined concrete block in compression zone. Frontiers of Structural and Civil Engineering, 2023, 17(10): 1585–1598
32. Bui L V H, Nguyen P T. Shear strength model of the reinforced concrete beams with embedded through-section strengthening bars. Frontiers of Structural and Civil Engineering, 2022, 16(7): 843–857
33. Elsamak G, Ghalla M, Badawi M, Albogami A, Tawfik T A, Shahin R I. Anchored and epoxied ferrocement strips for improving flexural performance of two-way reinforced concrete slabs. Case Studies in Construction Materials, 2025, 22: e04314
34. Askar M K, Hassan A F, Al-Kamaki Y S S. Flexural and shear strengthening of reinforced concrete beams using FRP composites: A state of the art. Case Studies in Construction Materials, 2022, 17: e01189
35. Godat A, Hammad F, Chaallal O. State-of-the-art review of anchored FRP shear-strengthened RC beams: A study of influencing factors. Composite Structures, 2020, 254: 112767
36. Baggio D, Soudki K, Noël M. Strengthening of shear critical RC beams with various FRP systems. Construction and Building Materials, 2014, 66: 634–644
37. Shomali A, Mostofinejad D, Esfahani M R. Experimental and numerical investigation of shear performance of RC beams strengthened with FRP using grooving method. Journal of Building Engineering, 2020, 31: 101409
38. Saribiyik A, Abodan B, Balci M T. Experimental study on shear strengthening of RC beams with basalt FRP strips using different wrapping methods. Engineering Science and Technology, an International Journal, 2021, 24(1): 192–204
39. Elsamak G, Fayed S. Flexural strengthening of RC beams using externally bonded aluminum plates: an experimental and numerical study. Advances in Concrete Construction, 2021, 11: 481–492
40. Sundarraja M C, Rajamohan S. Strengthening of RC beams in shear using GFRP inclined strips—An experimental study. Construction and Building Materials, 2009, 23(2): 856–864
41. Täljsten B. Strengthening concrete beams for shear with CFRP sheets. Construction and Building Materials, 2003, 17(1): 15–26
42. Gonzalez-Libreros J H, Sneed L H, D'Antino T, Pellegrino C. Behavior of RC beams strengthened in shear with FRP and FRCM composites. Engineering Structures, 2017, 150: 830–842
43. Tetta Z C, Koutas L N, Bournas D A. Textile-reinforced mortar (TRM) versus fiber-reinforced polymers (FRP) in shear strengthening of concrete beams. Composites. Part B, Engineering, 2015, 77: 338–348
44. Al-Salloum Y A, Elsanadedy H M, Alsayed S H, Iqbal R A. Experimental and numerical study for the shear strengthening of reinforced concrete beams using textile-reinforced mortar. Journal of Composites for Construction, 2012, 17(1): 74–90

45. Emara M, Torres L, Baena M, Barris C, Moawad M. Effect of sustained loading and environmental conditions on the creep behavior of an epoxy adhesive for concrete structures strengthened with CFRP laminates. Composites Part B Engineering, 2017, 129: 88–96
46. Emara M, Elkomy N, Hassan H. Numerical assessment of reinforced concrete beams strengthened with CFRP sheets under impact loading. Frattura Ed Integrità Strutturale, 2021, 15(58): 48–64
47. Ng C K. Tendon stress and flexural strength of externally prestressed beams. ACI Structural Journal, 2003, 100(5): 644–653
48. Ng C K, Tan K H. Flexural behaviour of externally prestressed beams Part I: Analytical model. Engineering Structures, 2006, 28(4): 609–621
49. Wang X, Shi J, Wu G, Yang L, Wu Z. Effectiveness of basalt FRP tendons for strengthening of RC beams through the external prestressing technique. Engineering Structures, 2015, 101: 34–44
50. Tan K H, Al Farooq M A, Ng C K. Behavior of simple-span reinforced concrete beams locally strengthened with external tendons. ACI Structural Journal, 2001, 98(2): 174–183
51. Lou T, Lopes S M R, Lopes A V. Numerical analysis of behaviour of concrete beams with external FRP tendons. Construction and Building Materials, 2012, 35: 970–978
52. Baraghith A T, Mansour W, Behiry R N, Fayed S. Effectiveness of SHCC strips reinforced with glass fiber textile mesh layers for shear strengthening of RC beams: Experimental and numerical assessments. Construction and Building Materials, 2022, 327: 127036
53. Khalil A E H A, Atta A M, Baraghith A T, Behiry R N, Soliman O E. Shear strengthening of concrete deep beams using pre-fabricated strain-hardening cementitious composite plates. Engineering Structures, 2023, 278: 115548
54. Hassan A, Atta A M, El-Shafiey T F. Restoration of the shear capacity for RC beams with web openings using precast SHCC plates. Structures, 2020, 25: 603–612
55. Ghalla M, Bahrami A, Badawi M, Mlybari E A. Novel sustainable techniques for enhancing shear strength of RC beams mitigating construction failure risk. Ain Shams Engineering Journal, 2024, 15(11): 103017
56. Bahrami A, Ghalla M, Elsamak G, Badawi M, Mlybari E A, Abdelmgeed F A. Various configurations of externally bonded strain-hardening cementitious composite reducing shear failure risk of defected RC beams. Frontiers in Materials, 2024, 11: 1373292
57. Elsamak G, Abdullah A, Salama M I, Hu J W, El-Mandouh M A. Punching shear behavior of slabs made from different types of concrete internally reinforced with SHCC-filled steel tubes. Materials, 2022, 16(1): 72
58. Salama M I, Hu J W, Almaadawy A, Hamoda A, Rageh B O, Elsamak G. Behavior of simple precast high-strength concrete beams connected in the maximum bending moment zone using steel extended endplate connections. Steel and Composite Structures, 2024, 50: 627
59. Hamoda A, El-Mandouh M A, Ahmed M, Abadel A A, Liang Q Q, Elsamak G. Experimental and numerical studies of reinforced concrete stair beams strengthened with steel bars and plates. Engineering Structures, 2023, 297: 117037
60. Hibbitt, Karlsson & Sorensen, Inc. ABAQUS Theory Manual, User Manual and Example Manual, Version 6.7, 2000
61. Heneash U, Ghalla M, Tawfik T A, Elsamak G, Emara M, Basha A. Impact of various dowel bars techniques in joints of plain concrete connected rigid pavements: Experimental and numerical investigations. Results in Engineering, 2025, 25: 103858
62. Emara M, Ghalla M, Hu J W, Badawi M, Mlybari E A, Ahmed S O. Enhancement of cantilevered RC beams exhibiting inadequate lap spliced reinforcement using sustainable reinforced ECC layers. Construction and Building Materials, 2024, 428: 136272
63. Badawi M, Bahrami A, Ghalla M, Emara M, Mlybari E A, Elsamak G. Flexural strengthening of reinforced concrete cantilever beams having insufficient splice length. Results in Engineering, 2024, 24: 102869
64. Ghalla M, Badawi M, Elsamak G, Ahmed M, Liang Q Q, El-Zareef M A. Strengthening of reinforced concrete beams with insufficient lapped splice length of reinforcing bars. Engineering Structures, 2024, 321: 118922
65. Hamoda A, Eltaly B, Ghalla M. Numerical investigation on reinforced concrete closed curved beams subjected to internal pressure strengthened with sustainable material. ERJ Engineering Research Journal, 2023, 46(2): 233–247
66. Hamoda A, Ghalla M, Yehia S A, Ahmed M, Abadel A A, Baktheer A, Shahin R I. Experimental and numerical investigations of the shear performance of reinforced concrete deep beams strengthened with hybrid SHCC-mesh. Case Studies in Construction Materials, 2024, 21: e03495
67. Carreira D J, Chu K H. Stress–strain relationship for plain concrete in compression. Journal Proceedings, 1985, 82(6): 797–804
68. Emara M, El-Zohairy A, Fekry M, Husain M. Effect of using ECC layer on the flexural performance of RC beams previously strengthened with EB CFRP laminates. Sustainability, 2022, 14(24): 16990
69. Ghalla M, Badawi M, Hu J W, Elsamak G, Mlybari E A, Emara M. Ultimate performance of two-way reinforced concrete flat slabs enhanced by SHCC drop panels mitigating punching failure. Journal of Building Engineering, 2025, 99: 111574
70. Salama M I, Elayat A, Reda M, Elsamak G. Influence of concrete type on rigid pavement behavior under static loads. Innovative Infrastructure Solutions, 2024, 9(1): 15
71. Elsamak G, Elmasry A H, Rageh B O. Numerical modelling of the behavior of bare and masonry-infilled steel frames with different types of connections under static loads. Computers and Concrete, 2024, 33: 103–119
72. Hekal G M, Salama M I, Elsamak G, Almaadawy A H. Shear behavior of RC beams strengthened with ultra-high-performance fiber-reinforced concrete using finite-element analysis. Asian Journal of Civil Engineering, 2023, 24(1): 71–91
73. Elsamak G, Ghalla M, Hu J W, Albogami A, Emara M, Ahmed S O. Embedded aluminum sections and prestressed high-performance concretes for improving shear performance of RC beams. Case Studies in Construction Materials, 2025, 22: e04168
74. Ghalla M, Badawi M, Mlybari E A, Hu J W. Enhancing shear strength of RC beams through externally bonded reinforcement with stainless-steel strips and FRCM jacket to mitigate the failure risk. Results in Engineering, 2024, 22: 102246